# Phenomenological Modeling of Fusion Welding Processes

S.A. David, T. DebRoy, and J.M. Vitek

## Introduction

Welding is utilized in 50% of the industrial, commercial, and consumer products that make up the U.S. gross national product.[1] In the construction of buildings, bridges, ships, and submarines, and in the aerospace, automotive, and electronic industries, welding is an essential activity. In the last few decades, welding has evolved from an empirical art to a more scientifically based activity requiring synthesis of knowledge from various disciplines. Defects in welds, or poor performance of welds, can lead to catastrophic failures with costly consequences, including loss of property and life.

Figure 1 is a schematic diagram of the welding process showing the interaction between the heat source and the base metal. During the interaction of the heat source with the material, several critical events occur: melting, vaporization, solidification, and solid-state transformations. The weldment is divided into three distinct regions: the fusion zone (FZ), which undergoes melting and solidification; the heat-affected zone (HAZ) adjacent to the FZ, that may experience solid-state phase changes but no melting; and the unaffected base metal (BM).

Creating the extensive experimental data base required to adequately characterize the highly complex fusion welding process is expensive and time consuming, if not impractical. One recourse is to simulate welding processes either mathematically or physically in order to develop a phenomenological understanding of the process. In mathematical modeling, a set of algebraic or differential equations are solved to obtain detailed insight of the process. In physical modeling, understanding of a component of the welding process is achieved through experiments designed to avoid complexities that are unrelated to the component investigated.

In recent years, process modeling has grown to be a powerful tool for understanding the welding process. Using computational modeling, significant progress has been made in evaluating how the physical processes in the weld pool influence the development of the weld pool and the macrostructures and microstructures of the weld. Much recent research on weld-pool phenomena has attempted to gain an understanding of fluid flow and heat transfer in the weld pool. In addition to information on weld-pool shape and size, computational modeling of the welding process can provide detailed information on such parameters as the weld cooling rate, temperature gradients, microstructural development, and residual stresses in the welded structures. Limited progress has also been made in modeling and understanding weld-pool solidification behavior and solid-state phase transformations in the FZ and the HAZ. Finally, process modeling has been used as a critical element for the intelligent control and automation of the welding process, to make welds with a desired quality, performance, and productivity.

A recent publication,[2] a series of international conferences,[3–6] and a recent workshop[7] have all covered the current issues, trends, and directions in weld process modeling. This article aims to provide a phenomenological perspective of modeling activities in fusion welding. A few examples, taken mostly from the authors' laboratories, highlight several important issues.

## Heat and Mass Transfer, and Fluid Flow

### Driving Forces for Motion

During fusion welding, the metal in the weld pool undergoes vigorous recirculatory motion driven by surface tension, buoyancy and, when electric current is used, electromagnetic forces.[8–13] Buoyancy effects originate from the spatial variation of the liquid metal density, mainly because of temperature variations and, to a lesser extent, from local composition variations. Electromagnetic effects are a consequence of the interaction between the divergent current path in the weld pool and the magnetic field it generates. The effect is important when a large electric current passes through the weld pool, as is the case for arc welding and electron-beam welding. Spatial variation of the surface tension, arising from temperature and composition gradients at the weld-pool surface, often provides the main driving force for the convective flow, known as the Marangoni flow. Fluid flow and heat transfer are important in determining the size and shape of the weld pool, the weld macrostructure and microstructure, and the weldability of the material.

### Flow Velocities in the Weld Pool

Frequently, the main driving force for convection is the spatial gradient of surface tension at the weld-pool surface. In most cases, the difference in surface tension arises from the temperature variation at the weld-pool surface. For such a situation, the Marangoni stress can be expressed as:

$$\tau = \frac{d\gamma}{dT}\frac{dT}{dr} \tag{1}$$

where $\tau$ is the shear stress due to the temperature gradient, $\gamma$ is the interfacial tension, $T$ is the temperature, and $r$ is the distance along the surface from the axis of the heat source. If a boundary layer develops, $\tau$ can be expressed as:[14]

$$\tau \approx \frac{0.664\rho^{1/2}\mu^{1/2}u_m^{3/2}}{W^{1/2}} \tag{2}$$

where $\rho$ and $\mu$ are the density and viscosity, $u_m$ is the local velocity, and $W$ is the width of the pool. The shear stress on the surface halfway between the heat source axis and the weld-pool edge is approximately the maximum stress, and the order of magnitude of the maximum velocity can be calculated from:

$$u_m^{3/2} \approx \frac{d\gamma}{dT}\frac{dT}{dr}\frac{W^{1/2}}{0.664\rho^{1/2}\mu^{1/2}} \tag{3}$$

For typical values of pool width of 0.5 cm, metal density of 7.2 g/cm$^3$, viscosity of 0.06 poise, temperature coefficient of surface tension, $d\gamma/dT$, of 0.5 dynes/(cm°C), and spatial gradient of temperature of 600°C/cm, the maximum velocity is approximately 62 cm/s. Considering that the weld pool is only 0.5 cm wide, this velocity is rather large. Even larger computed velocities of the order of 100 cm/s have been

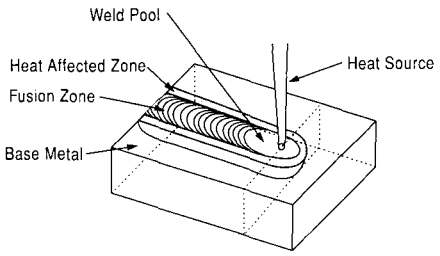


*Figure 1. Schematic diagram of the welding process showing the interaction between the heat source and the base metal.*

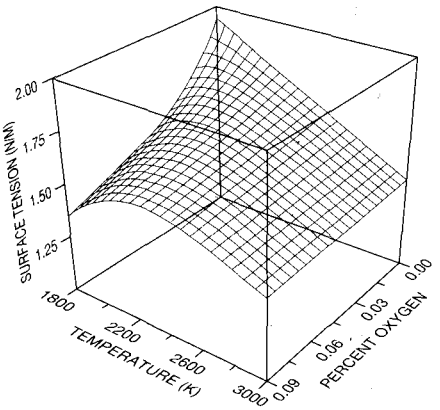


*Figure 2. Surface tension of Fe-O alloy as a function of temperature and oxygen concentration.[17,19]*

reported[12,13] in systems dominated by Marangoni convection. When the velocities are small, the shear stress, $\tau$, cannot be estimated by Equation 2, which is based on the boundary layer theory. For such a situation, a rough estimate of the shear stress can be obtained from geometric consideration as $2\mu u_m/d$, where $d$ is the depth of the weld pool. The expression for the approximate value of the maximum velocity can be obtained by combining this expression for shear stress with the expression for Marangoni stress, i.e., Equation 1. When the surface tension gradient is not the main driving force, the maximum velocities can be much smaller. For example, when the flow occurs primarily by natural convection, the maximum velocity, $u_m$, can be approximated by the following relation:[11]

$$u_m \approx \sqrt{g\beta\Delta T d} \qquad (4)$$

where $g$ is the acceleration due to gravity, $\beta$ is the coefficient of volume expansion, $\Delta T$ is the temperature difference that drives the flow, and $d$ is the depth. For typical values of $\Delta T = 600°C$, $g = 981$ cm/s$^2$, $\beta = 3.5\times10^{-5}$/°C, and $d = 0.5$ cm, the value of $u_m$ is 3.2 cm/s. Similar calculations can be done for electromagnetically driven flow. The magnitude of the velocities for both buoyancy and electromagnetically driven flows in the weld pool are commonly much smaller than those obtained for surface tension driven flows.

### Relative Importance of Heat Conduction and Convection

The relative importance of conduction and convection in the overall transport of heat in the weld pool can be assessed from the value of the Péclet number, which is given by:

$$\mathrm{Pe} = \frac{u\rho c_p L}{k} \qquad (5)$$

where $u$ is the flow velocity, $\rho$ is the density, $c_p$ is the specific heat at constant pressure, $L$ is the characteristic length and $k$ is the thermal conductivity of the melt. For a typical case with $u = 10$ cm/s, $\rho = 7.2$ g/cm$^3$, $c_p = 0.2$ cal/(g°C), $L = 0.5$ cm, and $k = 0.1$ cal/(cm s°C), the Pe is 72. When the Péclet number is this large, heat transport occurs primarily by convection, and conduction is not important. However, for metals with high thermal conductivity, at low velocities and for small pool sizes, the value of Pe can be low, and accurate calculations of heat transfer can be done using relatively simple conduction calculations. It should be noted that the conduction of heat in the solid region is important in the dissipation of heat away from the weld pool. Therefore, the thermal conductivity of the solid and the specimen dimensions are important in determining the size of the molten pool.

### Convection Effects on Weld-Pool Shape and Size

Variable depth of penetration during the welding of different heats of commercial material with the composition within a prescribed range has received considerable attention. The penetration depth is often determined by the concentration of the surface active elements in the commercial alloy.[12,15-18] These elements can affect the temperature coefficient of surface tension, $d\gamma/dT$, and the resulting direction of fluid flow in the weld pool[12] and the shape of the weld pool. The interfacial tension in these systems can be described[17,18] by a formalism based on the combination of Gibbs and Langmuir adsorption isotherms:

$$\gamma = \gamma_m^0 - A(T - T_m) - RT\Gamma_s \ln(1 + k_1 a_i e^{-\Delta H^0/RT}) \qquad (6)$$

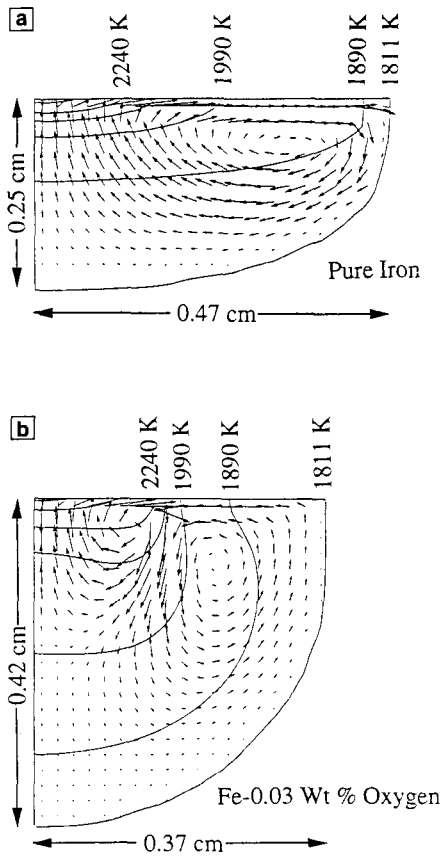


*Figure 3. Velocity and temperature fields for two different cases: (a) pure iron and (b) iron with 0.03 wt% oxygen.[19]*

where $\gamma$ is the interfacial tension as a function of composition and temperature, $\gamma_m^0$ is the interfacial tension of the pure metal at the melting point, $T_m$, $A$ is a constant, $R$ is the gas constant (in appropriate units), $T$ is the absolute temperature, $\Gamma_s$ is the surface excess of the solute at saturation solubility, $k_1$ is the entropy factor, $a_i$ is the activity of the solute, and $\Delta H^0$ is the enthalpy of segregation. The calculated values of surface tension[17,19] for Fe-O alloys are presented in Figure 2. It is observed that for high concentrations of oxygen, $d\gamma/dT$ can change from a positive value at "low" temperature to a negative value at "high" temperature. This implies that in a weld pool with a fairly high oxygen content, $d\gamma/dT$ can go through a change in sign on the surface of the pool. Under these conditions, the fluid flow in the weld pool is more complicated than a simple recirculation.

The calculated gas-tungsten arc (GTA) fusion zone profiles[19] for pure iron, and an iron-0.03 wt% oxygen alloy are presented

in Figure 3. The results in Figure 3 clearly show the significant effect of oxygen concentration on the weld-pool shape and the aspect ratio. Near the heat source, where the temperature is very high, the flow is radially outward. However, for the Fe-O alloy, a short distance away from the heat source where the temperature drops below the threshold value for the change in the sign of $d\gamma/dT$, the flow reverses direction. The flow field is not a simple recirculation. The computed values of the aspect ratio are compared with the experimental data of Heiple and Roper[20] for a stainless steel in Figure 4. Although there are only limited experimental data, good agreement is achieved between the calculated results and the experimental data. Similar behavior was observed[22,23] for the GTA fusion welding of 304 stainless steel containing 240 ppm sulfur. Apart from the good agreement between the experimental and the calculated weld-pool shapes, the calculations reveal new insights about the complexity of the flow field. Although the qualitative effects of the role of surface active elements were known, the numerical calculations provide a basis for quantitative assessment of their role in the development of the weld-pool geometry.

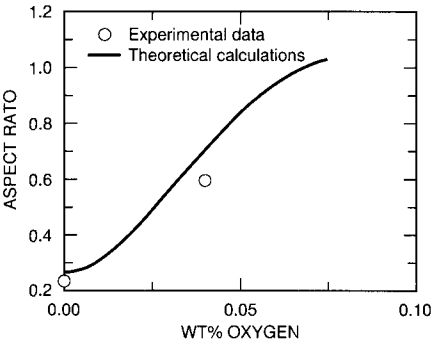


*Figure 4.Comparison of the predicted and experimental aspect ratios (depth to width).[19] The oxygen concentration of 0.04 wt% is obtained from the Cr-O equilibrium data for 21% Cr, given in Reference 21.*

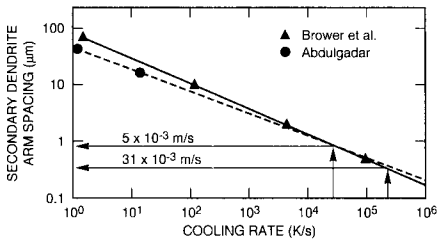


*Figure 5. Plot of secondary dendrite arm spacing as a function of cooling rate for conduction mode laser welding of AISI 201 stainless steel.[12]*

## Cooling Rate and Simple Features of Solidification Structure

The cooling rate at a given monitoring location is the product of the temperature gradient and the solidification growth rate. For several alloys, the secondary dendrite arm spacings have been experimentally correlated with the cooling rates. Therefore, using numerically computed cooling rates and the available experimental correlation, the secondary dendrite arm spacing can be estimated. In Figure 5, the computed secondary dendrite arm spacings of 0.9 $\mu$m and 0.4 $\mu$m for 5 mm/s and 31 mm/s welding speeds, respectively, are compared with the experimental data.[12] The good agreement between the predicted secondary dendrite arm spacing and the values obtained from independent experimental data demonstrates that the calculated values of cooling rates are fairly accurate. In another investigation[13] of the effect of pulsed laser welding on the thermal response of 310 and 316 austenitic stainless steels, the cooling rates were theoretically calculated from fundamental principles of transport phenomena. The secondary dendrite arm spacings were determined from the microstructures. The results indicated excellent agreement between the measured and the expected secondary dendrite arm spacings based on the cooling rates. The investigations with both continuous[12] and pulsed[13] heat sources indicate that simple features of the solidification structure can be determined from the available numerical models of weld-pool transport phenomena.

## Evaporation from Weld-Pool Surface

The weld-pool surface temperatures are normally much higher than the melting points of the weld metals. Consequently, pronounced vaporization of alloying elements takes place, especially when high-energy-density heat sources are used.[24–33] Such losses often result in a change in the composition of the weld metal, affect weld properties, and are a serious problem in the welding of many important engineering alloys.

Block-Bolten and Eagar[31] suggested that the weld-pool peak temperature is limited by the evaporation of elements from the weld pool. To determine the maximum temperature of the weld pool, they used the following energy balance.

$$W(T)\,[L_e - \Delta\overline{H}] = xP \qquad (7)$$

where $W(T)$ is the temperature-dependent vaporization rate, $L_e$ is the enthalpy of vaporization, $\Delta\overline{H}$ is the enthalpy of mixing, $P$ is the power density, and $x$ is the fraction of the input power used for vaporization. In Equation 7, $W(T)$ is computed from known values of all other parameters. Subsequently, the maximum temperature is determined from the known $W(T)$ versus $T$ relation. Their calculations indicated that the peak temperature for an iron-based alloy is about 2773 K for arc welding, and as high as 4273-5273 K for laser and electron beam welding. The relation between the vaporization rate $W(T)$ and the temperature, $T$, significantly affects the value of the temperature calculated from Equation 7. In fact, the temperature versus vaporization rate relation used by Block-Bolten and Eagar,[31] i.e. the Langmuir equation,[34] grossly overpredicts the vaporization rate at any given temperature, and likewise, for a given vaporization rate, it grossly underpredicts the temperature. Kraus[35] has shown that the peak temperature in GTA stainless steel welds, measured by the laser reflectance method, could reach as high as 2950 K. Thus, an appropriate correlation between the vaporization rate and the weld-pool temperature is essential for realistic calculations.

DebRoy et al.[25–27] developed a comprehensive mathematical model to understand vaporization of elements and the composition change of the weld metal. The computed weld-pool temperature distribution was used for the vaporization rate calculations. The weld-pool heat transfer and fluid flow were solved simultaneously with the velocity distribution functions of vapor molecules at various locations above the weld-pool surface to calculate the rates of vaporization of the alloying elements. The procedure allowed for the calculation of both the evaporation and condensation fluxes based on the application of conservation of mass, momentum, and energy equations in the gas phase.

A key feature of the calculations is the consideration of the pressure-gradient-driven mass transfer.[25–27,36,37] In laser processing of metals and alloys, the peak temperature reached at the surface often exceeds the boiling point of the irradiated material.[38–40] At temperatures higher than the boiling point, the pressures in the vicinity of the pool are greater than the ambient pressure, and the excess pressure provides a driving force for the vapor to move away from the surface. In addition, mass transfer rates due to concentration gradients were determined using available correlations among various dimensionless numbers.[41] Heat transfer to the shielding gas and heat loss due to vaporization of the

alloying elements were taken into account in the calculations. The calculated rates agreed well with the experimental data for the welding of pure iron and titanium, and for both low- and high-power $CO_2$ laser welding of 201 stainless steel. Straightforward calculations using the Langmuir equation do not account for the condensation of vapors. As a result, as noted previously, the rates calculated from the Langmuir equation are commonly much higher than the experimentally observed values. The calculated vaporization rates are significantly better than the corresponding values obtained from the straightforward application of the Langmuir equation. However, the higher accuracy achieved by including a more realistic and detailed description of the physical processes requires more complex calculations.

### *Physical Modeling of Nitrogen, Oxygen, and Hydrogen Partitioning*

The nitrogen, oxygen, and hydrogen concentrations in the weld metal strongly influence the microstructure and properties. The gases dissolve in the weld metal, whereupon they may form porosity or combine with alloying elements to form inclusions. For example, in the welding of steel, hydrogen induces cracking, nitrogen improves the tensile properties, and oxygen promotes inclusion formation. Therefore, reliable modeling of the partitioning of gases into the liquid metal is required.

When a metal is exposed to a pure diatomic gas such as hydrogen, the equilibrium concentration of the species in the metal is proportional to the square root of its partial pressure at any given temperature. This relation, known as the Sieverts' Law, is widely used for calculating solute concentrations in metals in equilibrium with diatomic gases. However, such estimations are not useful for most welding processes. Near the weld-pool surface, besides common diatomic molecules, also present within the gas plasma are excited molecules, atoms, and ions. As a result, the interstitial concentrations in the weld metal are significantly higher than those calculated from Sieverts' Law[42-47] The presence of excited neutral atoms, ions, and electrons[48,49] precludes any simple extension of the well-established formal treatment of gas-metal systems to welding. Efforts to develop a general principle for understanding the partitioning of nitrogen, oxygen, and hydrogen between the weld pool and its environment are just in their infancy.

Appropriately designed physical simulation of gas dissolution in the weld pool can avoid both temperature and composition gradients on the weld-pool surface and in the gas phase. Bandopadhyay et al.[47] conducted physical simulation experiments of nitrogen dissolution in the weld pool. They exposed drops of tantalum and niobium to controlled plasma environments with known concentrations of nitrogen in the feed gas. The plasma parameters were optically monitored during experiments. They observed significantly higher nitrogen solubilities in pure tantalum and niobium than those predicted by Sieverts' Law. The formation of excited neutral atoms in the gas phase by various inelastic electron impact reactions was found to be the main cause of enhanced nitrogen solubility.

## Weld Solidification

Development of the microstructure in the FZ, also known as weld metal, depends on the solidification behavior of the weld pool. Solidification behavior controls the size and shape of grains, the extent of segregation, and the distribution of inclusions and defects such as porosity and hot cracks. Since the properties and performance of the FZ depend on the solidification behavior and the microstructural characteristics, understanding weld-pool solidification behavior is essential. Efforts are under way to use both analytical and numerical models to better understand the solidification behavior of the FZ.[50-57] Most of our current knowledge of weld-pool solidification is derived from an extrapolation of the knowledge and models for freezing of castings, ingots, and crystals at lower thermal gradients and growth rates.[50] The same parameters that are important in determining microstructures in castings, such as growth rate ($R_S$), temperature gradient ($G$), undercooling ($\Delta T_U$), and alloy composition, play significant roles in determining the development of microstructures in welds. The temperature gradient and growth rate are important in the combined forms $G/R_S$ and $GR_S$ (cooling rate) since they influence the solidification morphology and the scale of the solidification substructure, respectively. In welding, where the molten pool is translated through the material, both $G$ and $GR_S$ vary considerably across the FZ. Depending on the type of welding process and the location within the weld pool, the maximum cooling rate encountered within the weld pool may range from $10^2$ to $10^7$°C/s. Experimental measurement of these parameters during welding is extremely difficult. Modeling can provide a reasonable alternative to direct measurements by allowing thermal gradients, growth rates, and cooling rates in the weld pool to be calculated.

Solidification microstructures found in welds are often quite complex. However, development of these microstructures can be understood by considering classical nucleation and growth theory. In welds, since solidification proceeds from the preexisting solid substrate, there is little or no nucleation barrier. Solidification occurs spontaneously by epitaxial growth. When a filler metal is used, in addition to epitaxial growth, the more classical case of heterogeneous nucleation may also apply. The stability of the solid-liquid interface is critical in determining the microstructural characteristics of the FZ. Conditions in the immediate vicinity of the interface determine whether the growth is planar, cellular, or dendritic. Theories have been developed for interface stability under conditions of equilibrium at the interface for normal solidification or under extreme nonequilibrium conditions that exist during rapid solidification.[58,59] Further, in recent years significant advances have been made in the theory and fundamentals of dendritic solidification.[60,61] These theories and models can be readily extended to weld-pool solidification.

In alloy solidification, where partitioning of solute elements between the solid and liquid occurs, the effects of solute redistribution and buildup at the solid-liquid interface on the morphological stability of the solidification front can be understood by considering the simple concept of constitutional supercooling.[58,59] This criterion for solidification-front instability can be mathematically stated as:

$$\frac{G_L}{R_S} < \frac{\Delta T_0}{D_L} \tag{8}$$

or, equivalently,

$$\frac{G_L}{R_S} < -\frac{M_L C_0(1 - K)}{KD_L} \tag{9}$$

where $G_L$ is the thermal gradient in the liquid at the solidification interface, $R_S$ is the solidification front growth rate, $M_L$ is the slope of the equilibrium liquidus line, $C_0$ is the overall alloy composition, $K$ is the equilibrium partition coefficient, $D_L$ is the solute diffusion coefficient in liquid, and $\Delta T_0$ is the equilibrium solidification temperature range at composition $C_0$. If this criterion is met, the planar solidification front is unstable and dendritic growth is promoted. If the reverse is true, namely $G_L/R_S > \Delta T_0/D_L$, then the plane front will be stable.

As growth conditions depart from planar stability, the interface morphology will change from planar to cellular to dendritic. If conditions are favorable, the dendrites will exhibit secondary and tertiary

branches as shown in Figure 6. The analysis that led to the theory of constitutional supercooling was not rigorous, and more thorough analyses have been carried out and additional conditions for plane front solidification have been developed.[62–67] As a result, an absolute stability region, where planar growth prevails, is predicted at high solidification rates as well at low rates. This latter morphological regime may be important for welds made at high speeds using high-energy beam processes.

Partitioning of solute between solid and liquid results in extensive solute redistribution during alloy solidification, and this can significantly affect weldability, microstructure, and properties. Both microsegregation (on a fine scale of the order of the dendrite arm spacing) and macrosegregation (on a large scale of a few hundred microns to millimeters) may occur in welds. Attempts have been made to characterize and model solute redistribution during weld-pool solidification.[30,55,68,69] These studies have extended different models used to describe the solute redistribution and the resulting segregation in castings and single crystals to welding situations. Here one must consider redistribution in front of the dendrite tip as well as within the interdendritic regions (also known as the mushy zone). Solute redistribution in the mushy zone of a weld can be modeled by applying principles originally formulated for castings. Many of the approaches used to model microsegregation start with the simple Scheil equation[70] that describes the composition of the solid as a function of the fraction that is solid in a representative volume element in the mushy zone:

$$C_S^* = KC_0(1 - f_S)^{k-1} \quad (10)$$

where $C_S^*$ is the solid composition, $C_0$ is the overall alloy composition, $K$ is the partition coefficient, and $f_S$ is the volume fraction that is solid. Significant advances have been made in modifying this model to account for limited or extensive diffusion in the solid.[71,72] In estimating the extent of segregation in welds, it is not adequate to consider the solute redistribution in the weld mushy zone alone; it is also essential to consider the solute redistribution in front of the dendrite tips. The composition at the dendrite tip is determined by the dendrite tip temperature and the partition coefficient. The tip temperature, partition coefficient, and composition are strong functions of the tip radius, growth rate, thermal gradient, and other factors. The effect of increased undercooling at the dendrite tip, which may be present during welding, would be to decrease the degree of coring and thus decrease the extent of microsegregation. Some of these concepts have been tested and verified in welds.[55,68]

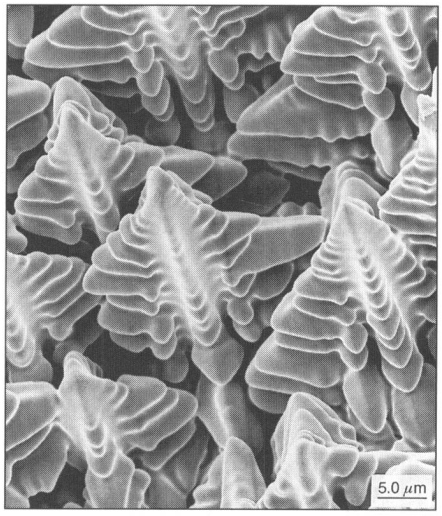


*Figure 6. Scanning electron micrograph showing the development of dendrites in a nickel-based superalloy single-crystal weld. The micrograph was taken on a hot-cracked surface formed during electron-beam welding of the alloy. The primary, secondary, and tertiary dendrite arms are clearly discernible.*

Another exciting area of research in welding is the understanding and modeling of grain structure development in the FZ. The development of the FZ grain structure in a weld is primarily controlled by the base metal grain structure and the welding conditions. As mentioned earlier, initial growth normally occurs epitaxially at the partially melted grains.[73–75] Both crystallographic effects and welding conditions can strongly influence the development of microstructure in the FZ. Specifically, crystallographic effects will influence grain growth by favoring growth along particular crystallographic directions—namely the easy growth directions.[58,59] For cubic metals, the easy growth directions are the family of ⟨100⟩ directions. Optimum growth conditions exist when one of the easy growth directions coincides with the heat flow direction. There is a strong interplay between the shape of the pool and growth crystallography. Limited progress has been made in our understanding of the development of grain structure in welds because it is difficult to interpret and understand fully the development of polycrystalline FZ microstructures. This is true since the details of the grain growth selection process and the three-dimensional pool shape are obscured by the multitude of grains and crystal orientations present in polycrystalline materials.

Welding experiments with single crystals have been found to be extremely useful in this situation. Recently, with the aid of single-crystal welds, significant advances have been made in understanding and modeling the interrelationships between weld-pool geometry, growth crystallography, and the dendrite selection process in the development of FZ microstructures.[51–54,57] This experimental technique has been found to be extremely powerful. Also, a geometrical model has been developed that enables prediction of the stable dendrite growth directions as a function of pool shape for various crystal orientations. The same model is being extended to evaluate the competitive dendrite growth behavior in bicrystal welds.[54] From the observed dendritic arrangements in the single-crystal welds, it is possible to reconstruct a three-dimensional weld pool shape as shown in Figure 7. The technique may serve as a tool to experimentally verify the pool shapes predicted by some of the computational models. Furthermore, the insight gained from such single-crystal weld experiments can be readily extended toward a better understanding of microstructural development in polycrystalline materials.

## Modeling Phase Transformations in Welds

During welding, extensive phase transformations occur in both the FZ and the HAZ. In addition to the solidification reaction, solid-state transformations may also take place. The nature of these transformations depends on the heating and cooling rates and also the maximum temperature reached at any given location during the weld thermal cycle. Modeling of these transformations and the resulting microstructures in weldments remains a great challenge. In the FZ, the extreme solidification conditions prevalent during many welding processes often lead to the solidification of nonequilibrium phases.[76,77] As described in a recent summary,[78] several investigators have tried to model the nonequilibrium solidification behavior in austenitic stainless steels using advanced solidification theories, thermodynamic analyses, and other methods. These analyses have, to date, met with only limited success.

Solid-state transformations may occur during post-solidification cooling in the FZ or in the HAZ. The HAZ, because of its extensive thermal gradient and nonuniform thermal exposure, may undergo widely different transformation character-

istics. As a result, the HAZ often exhibits significant compositional, microstructural, and property gradients. Such gradients are unique to welded structures. In addition, generation of thermal stresses during welding can drastically affect the kinetics of solid-state phase transformations in both the FZ and HAZ. Several advances have been made in recent years in modeling the solid-state phase transformations in weldments.[79–84] Models have been developed based on physical metallurgy principles. Efforts are also underway to use Monte Carlo techniques to simulate grain growth behavior in the HAZ and to quantitatively predict microstructural evolution in the HAZ.[85]

Phase transformations in weldments have a unique character that requires consideration of the transient heating as well as cooling to accurately understand the microstructural development. Therefore, traditional isothermal transformation kinetics and also cooling transformation kinetics must be supplemented by the inclusion of transformation effects during heating. This results in a combination of thermal histories, which are not commonly addressed in traditional studies, and it leads to additional complications. Any successful phase transformation modeling also requires a basic coupling with accurate thermal models. This coupling is critical for the development of a comprehensive, integrated model for the microstructural development in weldments.

## Residual Stresses

Stresses develop in welded structures because of non-uniform heating and structural changes. Residual stresses in weldments may produce distortion or cause premature failure in weldments or both.[86] Computational models can provide a detailed description of the residual stress distribution in weldments.[87–93] A prerequisite for the calculations is the detailed time-temperature history obtained from numerical calculations. Calculations of distortions, stresses, and strains are computationally intensive, and they take significantly more computer time than the calculation of the transient temperature field. Recently, the trend in these calculations has moved from cross-sectional two-dimensional plane strain and axisymmetric models to models using plane stress, shell, and three-dimensional elements.[90] Tekriwal and Mazumder[92] performed a three-dimensional thermomechanical analysis of the gas-metal arc welding to calculate distortions, stresses, and strains. Good qualitative agreement was achieved between the calculated and the measured transient strains. However, the calculated and measured residual strains were different. The differences were attributed to lack of an accurate stress-strain constitutive relation and the use of a coarse grid. Oddy et al.[93] showed that phase transformations can significantly affect the residual stresses generated by the welding of some steels. Thus, the uncertainties in the calculation procedures include the inaccuracies in the calculation of transient time-temperature history as well as the approximations in the assumed stress-strain relation, particularly when important solid-state transformations take place.

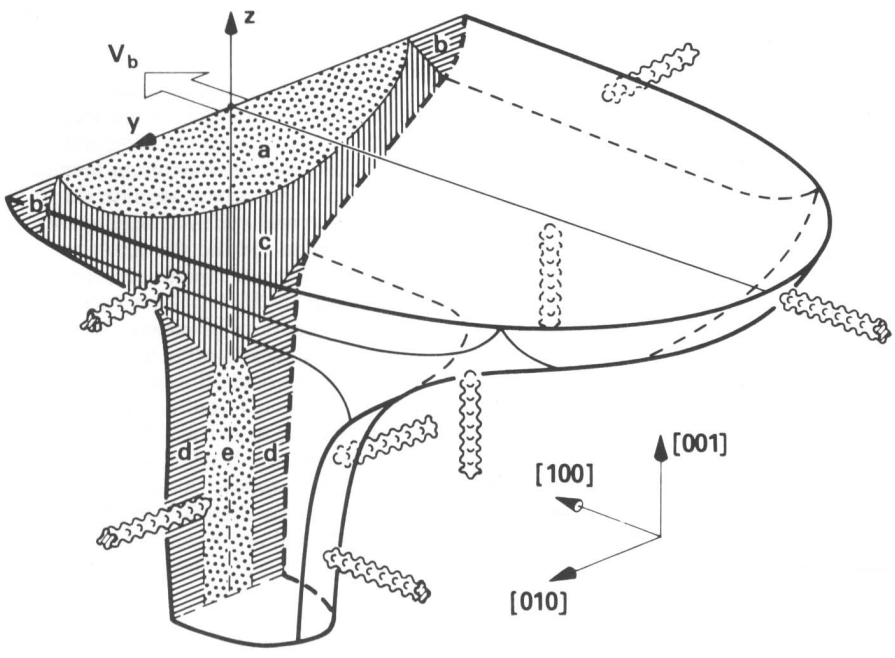


*Figure 7. Three-dimensional schematic diagram of a weld pool. The weld-pool shape was constructed using several two-dimensional transverse optical micrographs of Fe-15Cr-15Ni alloy single-crystal welds. $V_b$ represents the velocity of the heat source.*

## Epilogue

In recent years, modeling has provided significant insight into the dynamics of the welding process and the properties of welded materials which could not have been obtained otherwise. However, these accomplishments must be balanced against significant limitations of the work so far, and more importantly in perspective of what new avenues have been opened by the work that has been completed.

Because welding processes are so complex, modeling them is computationally intensive, expensive, and requires trained personnel. Although phenomenological modeling is a powerful tool, the modeling to date has been of limited use to practicing engineers because of its complexity, cost, and need for user training. Furthermore, most of the models have not been adequately standardized because the published works have focused on limited experimental verification. Therefore, standardization of the models would be a step toward gaining the greater confidence of practicing engineers. Improved user access to the models at low cost would also be helpful, if not essential, for gaining wider acceptance of the models in engineering practice.

Phenomenological modeling has an important role in developing adaptive control for obtaining defect-free welds. Implementation of adaptive control in welding would involve sensing and control of the heat source position, weld-pool temperature, weld penetration, defect formation, and, ultimately, would lead to control of microstructure and properties. An important element in the intelligent control loop is process modeling. Process modeling calculations in real time could provide the necessary bridge for coupling the process parameters with the desirable microstructure and properties of the weld. Most of the comprehensive phenomenological models require extensive computer time and cannot be used for real-time applications. However, these large models are essential for "calibrating" the computationally simpler models that can be used in real time. Such efforts would form a realistic basis for science-based control of

weld metal structure, composition, and properties.

## Acknowledgments

The authors wish to acknowledge helpful comments from Drs. S. Babu and S. Viswanathan. The research was sponsored by the Division of Materials Sciences, the U.S. Department of Energy, under contract DE-AC05-84OR21400 with Martin Marietta Energy Systems, Inc.; and grant DE-FG02-84ER45158 with Pennsylvania State University.

## References

1. American Welding Society Statement, *USA Today* (March 22, 1992).
2. S.A. David and T. DebRoy, *Science* **257** (1992) p. 497.
3. *Advances in Welding Science and Technology*, edited by S.A. David (ASM International, Materials Park, Ohio, 1986).
4. *Recent Trends in Welding Science and Technology*, edited by S.A. David and J.M. Vitek (ASM International, Materials Park, Ohio, 1990).
5. *International Trends in Welding Science and Technology*, edited by S.A. David and J.M. Vitek (ASM International, Materials Park, OH, 1993).
6. *Mathematical Modelling of Weld Phenomena*, edited by H. Cerjak and K.E. Easterling (The Institute of Materials, London, 1993).
7. Modeling for Welding Science, DOE-BES Workshop (Cocoa Beach, March 16–19, 1993).
8. S. Kou and Y. Le, *Metall. Trans. A* **14A** (1983) p. 2243.
9. G.M. Oreper and J. Szekely, *J. Fluid Mech.* **147** (1984) p. 53.
10. C. Chan, J. Mazumder, and M.M. Chen, *Metall. Trans. A* **15A** (1984) p. 2175.
11. J. Szekely in Reference 3, p. 3.
12. A. Paul and T. DebRoy, *Metall. Trans. B* **19B** (1988) p. 851.
13. T. Zacharia, S.A. David, J.M. Vitek, and T. DebRoy, *Metall. Trans. A* **20A** (1989) p. 957.
14. C.J. Geankoplis, *Transport Processes and Unit Operations* (Allyn and Bacon, Boston, 1983).
15. C.R. Heiple and J.R. Roper, *Weld. J. Res. Supp.* **61** (1982) p. 92s.
16. C.R. Heiple, J.R. Roper, R.T. Stagner, and J.J. Alden, in Reference 15, p. 72s.
17. P. Sahoo, T. DebRoy, and M.J. McNallan, in Reference 12, p. 483.
18. M.J. McNallan and T. DebRoy, *Metall. Trans. B* **22B** (1991) p. 557.
19. K. Mundra and T. DebRoy, unpublished research, Department of Materials Science and Engineering, Pennsylvania State University, University Park, PA.
20. R. Heiple and J.R. Roper, in *Trends in Welding Research*, edited by S.A. David, (ASM, Metals Park, OH, 1982) p. 489.
21. F.D. Richardson, *Physical Chemistry of Melts in Metallurgy*, Vol. 2 (Academic Press, London, 1974) p. 349.
22. T. Zacharia, S.A. David, J.M. Vitek, and T. DebRoy, *Weld. J. Res. Supp.* **68** (1989) p. 499s.
23. T. Zacharia, S.A. David, J.M. Vitek, and T. DebRoy, in Reference 22, p. 510s.
24. P.A.A. Khan and T. DebRoy, *Metall. Trans. B* **15B** (1984) p. 641.
25. T. DebRoy, S. Basu, and K. Mundra, *J. Appl. Phys.* **70** (1991) p. 1313.
26. K. Mundra and T. DebRoy, *Metall. Trans. B* **24B** (1993) p. 145.
27. K. Mundra and T. DebRoy, *Weld. J. Res. Supp.* **72** (1993) p. 1s.
28. T. DebRoy, in Reference 5, p. 17.
29. P.A.A. Khan, T. DebRoy, and S.A. David, *Weld. J. Res. Supp.* **67** (1988) p. 1s.
30. M.J. Cieslak and P.W. Fuerschbach, in Reference 12, p. 319.
31. A. Block-Bolten and T.W. Eager, in Reference 24, p. 461.
32. A. Blake and J. Mazumder, *J. Eng. Industry* **107** (1985) p. 275.
33. S. Basu, MS thesis, Pennsylvania State University, 1992.
34. R.D. Pehlke, *Unit Processes in Extractive Metallurgy* (Elsevier, New York, 1979).
35. H.G. Kraus, in Reference 22, p. 269s.
36. S.I. Anisimov and A.K. Rakhmatulina, *Sov. Phys. JETP* **37** (1973) p. 41.
37. C.J. Knight, *AIAA J.* **17** (1979) p. 519.
38. M. von Allmen, *Laser-Beam Interactions with Materials* (Springer-Verlag, Berlin, 1987).
39. V.A. Batanov, F.V. Bunkin, A.M. Prokhorov, and V.B. Fedorov, *Sov. Phys. JETP* **36** (1973) p. 311.
40. C.L. Chan and J. Mazumder, *J. Appl. Phys.* **62** (1987) p. 4579.
41. E.U. Schlunder and V. Gniclinski, *Chem.–Ing.–Tech.* **39** (1967) p. 578.
42. S.A. Gedeon and T.W. Eagar, *Weld. J. Res. Supp.* **69** (1990) p. 264s.
43. S. Ohno and M. Uda, *Trans. Nat. Res. Inst. Met.* **23** (1981) p. 243.
44. G. den Ouden and O. Griebling, in Reference 4, p. 431.
45. M. Uda, S. Ohno, and T. Wada, *J. Jpn. Weld. Soc.* **38** (1969) p. 382.
46. M. Uda and S. Ohno, *Trans. Nat. Res. Inst. Met.* **15** (1973) p. 20.
47. A. Bandopadhyay, A. Banerjee, and T. DebRoy, *Metall. Trans. B* **23B** (1992) p. 207.
48. G.J. Dunn and T.W. Eagar, *Metall. Trans. A* **17A** (1986) p. 1865.
49. M.M. Collur and T. DebRoy, *Metall. Trans. B* **20B** (1989) p. 227.
50. S.A. David and J.M. Vitek, *Intl. Materials Rev.* **34** (1989) p. 213.
51. M. Rappaz, S.A. David, J.M. Vitek, and L.A. Boatner, in Reference 13, p. 1125.
52. M. Rappaz, S.A. David, J.M. Vitek, and L.A. Boatner, *Metall. Trans. A* **21A** (1990) p. 1767.
53. S.A. David, J.M. Vitek, M. Rappaz, and L.A. Boatner, in Reference 52, p. 1753.
54. M. Rappaz, J.M. Vitek, S.A. David, and L.A. Boatner, *Metall. Trans. A* **24A** (1993) p. 1443.
55. J.A. Brooks, M.J. Baskes, and F.A. Greulich, *Metall. Trans. A* **22A** (1991) p. 915.
56. J.W. Elmer, T.W. Eagar, and S.M. Allen, in *Proc. Int'l. Conf. Stainless Steels* (Iron and Steel Institute of Japan, Tokyo, 1991) p. 669.
57. A. Matsunawa, S. Katayama, and M. Shimidzu, *Trans. Jpn. Weld. Res. Inst.* **19** (1990) p. 67.
58. M.C. Flemings, *Solidification Processing* (McGraw-Hill, New York, 1984).
59. W. Kurz and D.J. Fisher, *Fundamentals of Solidification* (Trans Tech Publications, Aedermannsdorf, Switzerland, 1986).
60. J.S. Langer, in *Principles of Solidification and Materials Processing*, Vol. 1, edited by R. Trivedi, J.A. Sekhar, and J. Mazumdar (Oxford & JBH Publishing Co., New Delhi, 1989) p. 1.
61. M.E. Glicksman, in Reference 60, p. 11.
62. W.W. Mullins and R.F. Sekerka, *J. Appl. Phys.* **35** (1964) p. 444.
63. R. Trivedi, *Acta Metall.* **18** (1970) p. 287.
64. W. Kurz and D.J. Fisher, *Acta Metall.* **29** (1981) p. 11.
65. W. Kurz, B. Giovanola, and R. Trivedi, *Acta Metall.* **34** (1986) p. 823.
66. R. Trivedi and W. Kurz, in Reference 65, p. 1663.
67. J.S. Langer and H. Müller-Krumbhaar, *Acta Metall.* **26** (1978) p. 1681.
68. J.A. Brooks and M.I. Baskes, in Reference 11, p. 93.
69. J.C. Lippold and W.F. Savage, *Modeling of Casting and Welding Processes*, edited by H.D. Brody and D. Apelian (Metallurgical Society of AIME, Warrendale, PA, 1980) p. 443.
70. E. Scheil, *Z. Metallk.* **34** (1942) p. 70.
71. H.D. Brody and M.C. Flemings, *Trans. AIME* **236** (1966) p. 615.
72. T.W. Clyne and W. Kurz, *Metall. Trans. A* **12A** (1981) p. 965.
73. W.F. Savage, *Weld. World* **18** (1980) p. 89.
74. G.J. Davies and J.G. Garland, *Int. Met. Rev.* **20** (1975) p. 83.
75. S.A. David and C.T. Liu, in Reference 15, p. 157s.
76. J.M. Vitek and S.A. David, *The Metal Science of Joining*, edited by M.J. Cieslak, J.H. Perepezko, S. Kang, and M.E. Glicksman (The Minerals, Metals, and Materials Society, Warrendale, PA, 1992) p. 115.
77. J.W. Elmer, in Reference 76, p. 123.
78. J.M. Vitek and S.A. David, in *Proc. Laser Processing Symposium* (The Minerals, Metals, and Materials Society, Warrendale, PA, 1993) to be published.
79. K.E. Easterling in Reference 6, p. 163.
80. H.K.D.H. Bhadeshia and L.E. Svensson, in Reference 79, p. 109.
81. H.K.D.H. Bhadeshia, *Bainite in Steels* (Institute of Materials, London, 1992).
82. H.K.D.H. Bhadeshia, in Reference 4, p. 189.
83. D.F. Watt, L. Coon, M. Bibby, J. Goldak, and C. Henwood, *Acta Metall.* **36** (1988) p. 3029.
84. C. Henwood, M. Bibby, J. Goldak, and D. Watt, in Reference 83, p. 3037.
85. Y. Shen, B. Radhakrishnan, and R.G. Thompson, in Reference 5, p. 259.
86. *Welding Handbook*, 8th ed., Chapter 7, K. Masubuchi, O.W. Blodgett, S. Matsui, F.P. Ross, C.O. Rudd, and C.L. Tsai (American Welding Society, Miami, FL, 1989).
87. J.K. Hepworth, *Finite Element Calculation of Residual Stresses in Welds*, (Proc. Int. Conf. Numerical Methods for Non-Linear Problems, Pineridge Prep, Swansea, Wales, September 1980) p. 51.
88. A.R. Ortega, L.A. Bertram, E.A. Fuchs, K. Mahin, and D.V. Nelson, in Reference 5, p. 89.
89. J.M.J. McDill, A.S. Oddy, and J.A. Goldak, in Reference 5, p. 105.
90. J. Goldak, in Reference 4, p. 72.
91. K.W. Mahin, W. Winters, J. Krafcik, T. Holden, R. Hosbons, and S. MacEwen, in Reference 4, p.83.
92. P. Tekriwal and J. Mazumder, in Reference 4, p. 91.
93. A.S. Oddy, J.A. Goldak, and J.M.J. McDill, in Reference 4, p. 97. □